Computer Modelling of Cyclic Deformation of High-Temperature Materials

TECHNICAL PROGRESS REPORT

Contract #N00014-91-C-0067

Dr. M.S. Duesbery
Principal Investigator

Dr. N.P. Louat
Senior Scientist

Fairfax Materials Research, Inc.
5613 Marble Arch Way
Alexandria, VA 22310-4011

February 26, 1993

Period of performance
November 16, 1992 through February 15, 1993

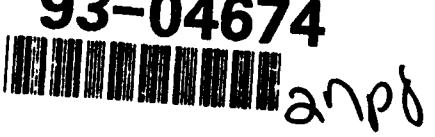

DISCLAIMER NOTICE

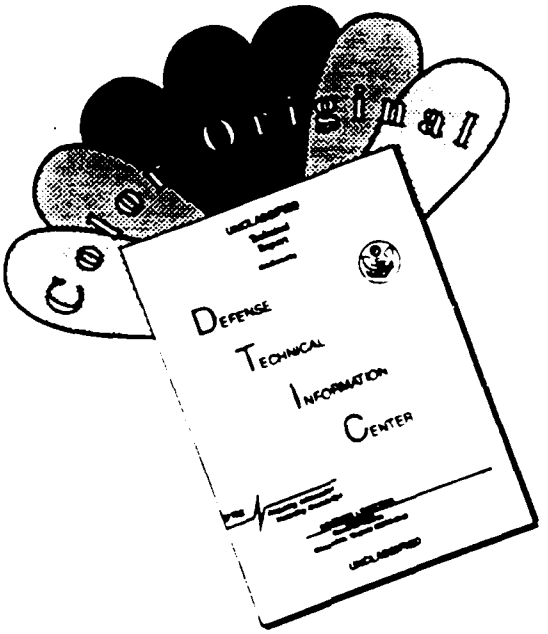

THIS DOCUMENT IS BEST QUALITY AVAILABLE. THE COPY FURNISHED TO DTIC CONTAINED A SIGNIFICANT NUMBER OF COLOR PAGES WHICH DO NOT REPRODUCE LEGIBLY ON BLACK AND WHITE MICROFICHE.

I. Introduction and Program Objective

Current methods of lifetime assessment leave much to be desired. Typically, the expected life of a full-scale component exposed to a complex environment is based upon empirical interpretations of measurements performed on microscopic samples in controlled laboratory conditions. Extrapolation to the service component is accomplished by scaling laws which, if used at all, are empirical; little or no attention is paid to synergistic interactions between the different components of the real environment. With the increasingly hostile conditions which must be faced in modern aerospace applications, improvement in lifetime estimation is mandated by both cost and safety considerations.

This program aims at improving current methods of lifetime assessment by building in the characteristics of the micro-mechanisms known to be responsible for damage and failure. The broad approach entails the integration and, where necessary, augmentation of the micro-scale research results currently available in the literature into a macro-scale model with predictive capability.

In more detail, the program will develop a set of hierarchically structured models at different length scales, from atomic to macroscopic, at each level taking as parametric input the results of the model at the next smaller scale. In this way the known microscopic properties can be transported by systematic procedures to the unknown macro-scale region. It may not be possible to eliminate empiricism completely, because some of the quantities involved cannot yet be estimated to the required degree of precision. In this case the aim will be at least to eliminate functional empiricism. Restriction of empiricism to the choice of parameters to be input to known functional forms permits some confidence in extrapolation procedures and has the advantage that the models can readily be updated as better estimates of the parameters become available.

II. Program Organization

The program has been organized into specific tasks and subtasks as follows.

Task 100. Lifetimes of metallic dispersed-phase composites

Most service materials fall into the category of dispersion-hardened metallic composites. This task will consider the problem of dispersion hardened materials in general, but with two specific materials, NiAl and $MoSi_2$/SiC in mind.

Task 110. Identification and modelling of micromechanisms

The purpose of this task is to determine what micromechanisms are operative in the high-temperature deformation of dispersion-hardened materials. In the general case this will be done by a literature search. For specific materials, the micromechanisms will be determined from the experimental program at NRL. Once identified, each of these micromechanisms will be

modelled, in order to determine what are the critical parameters which determine its effect on plastic flow and values for these parameters. Also to be determined is whether the modelled critical values are dependent on quantities which must be obtained from a smaller scale model.

Task 111. Equiaxed dispersoids

This task will consider dispersions of the type encountered in NiAl-like materials. That is, the dispersoids are considered to be small compared to the grain size. The term 'equiaxed' is used because the particles are roughly of the same size in all three dimensions. However, this is not a requirement for this task. Rather, it is necessary that the particles not be too large in the dimension normal to the slip plane, so that they can be surmounted with relative ease by cross-slip and/or climb without the generation of appreciable back-stress.

Task 112. Anisotropic dispersoids

This task covers the case of dispersoids which are elongated in the direction normal to the slip plane. An example is SiC fibers in $MoSi_2$. In this case, plastic flow around the dispersoids takes place by a combination of glide and climb, but is a protracted process during which large stresses acting in opposition to the applied load are developed.

Task 113. Grain boundary effects

This task will examine the role of grain boundary processes in high-temperature deformation.

Task 120. Macroscopic stochastic model for creep

In real materials it is likely that more than one mechanism will be operative, either in parallel or in series. The information gained in task 110 is not sufficient to describe this situation. Once the critical parameters for individual mechanisms have been determined, it is necessary to combine them in a macroscale stochastic model. This will be done by determining critical stresses and activation enthalpies as a function of local geometry and using these values in a finite-temperature simulation of creep through a random array of dispersoids. Careful attention must be paid to possible interactions between mechanisms.

Task 130. Extension to cyclic deformation

The final step in task 100 is to extend the results to the case of cyclic deformation. Irreversibility is an intrinsic feature of the model in task 120. However, it is likely that other, as yet unrecognized, characteristics of cycled deformation will have to be considered.

Task 200. Lifetimes of piezoelectric ferroelectrics

Failure in cyclic loading of sensors and actuators formed from lead zirconate titanate (PZT) is a continuing problem. PZT is a ceramic and therefore differs from the materials considered in

task 100 in that plastic deformation is not involved. This task will examine, modelling as necessary, the operation of PZT devices, in order to determine the factors governing lifetime limitation.

Task 300. Reporting

Running concurrently with tasks 100 and 200, this task will inform the Navy Program Manager and Contracting Officer of the technical and fiscal status of the program through R&D status reports.

III. Technical Progress

Task 120. Macroscopic stochastic model for creep

A numerical model has been developed to predict creep strengths and lifetimes for a metallic matrix with an arbitrary dispersion of second-phase particles of varying size and strength. An analytic treatment of the limiting case of impenetrable particles is given in the preprint reproduced in Appendix A.

a. Theory

a.1 Description of Model

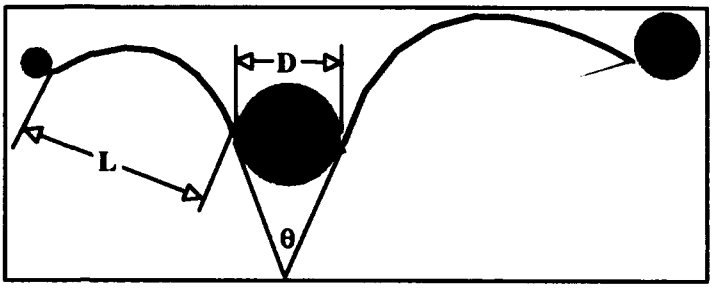

Figure 1 Definition of the geometric dispersion parameters D, L and θ

Figure 1 defines the parameters which describe the geometry of the general dispersion. Dispersoids (assumed to be spherical) intersect the slip plane in circles (shown in red in Figure 1) of different diameters, D_i, and are separated by distances L_{ij}. The angle between the dislocation arms at the ith dispersoid is θ_i. The value assumed by the angle θ at the point of Orowan looping defines the strength of the dispersoid, as described in the previous report[1]. An important feature of the model is that the mechanical properties of the dispersion, both athermal and thermal, are defined completely by the parameters L, D and θ[1]. To recapitulate, L and D define the line tension, T, of the dislocation, via the relations

$$T = A\frac{\mu b^2}{4\pi}\ln X \qquad \frac{1}{X} = \frac{1}{L} + \frac{1}{D} \qquad (1)$$

where μ is the shear modulus, b is the magnitude of the Burgers' vector and A is a constant with the value 1 for edge dislocations and $1/(1-\nu)$ for screw dislocations (ν is Poisson's ratio). The strength of the dispersoid is determined by the angle θ, by way of the expression

$$\tau bL = 2T\cos\frac{\theta}{2} \qquad (2)$$

in which τ is the effective stress. The left hand side of (2) represents the forward force on the dislocation, while the right hand side is the opposing force exerted by the dispersoid.

The formalism of (1) and (2) follows the generalization by Duesbery and Sadananda[2] of a model put forward by Bacon, Kocks and Scattergood[3] and has been shown to be compatible with a wide range of experimental observations[1].

Key *innovations* of the numerical model are as follows.

★Explicit temperature dependence in both strength and creep calculations is incorporated. The activation enthalpy for any dispersoid can be calculate by integrating the expression (2) with respect to θ from the equilibrium to the critical value.

★The estimation of lifetimes of order up to years from a model with a time scale of picoseconds is impractical. A novel algorithm has been developed which permits prediction of long-term creep properties from a microscale model. Knowledge of the activation enthalpy for each dispersoid along the dislocation line permits computation of the probability of activation. Combining this with the vibration frequency of the dislocation allows determination of the mean waiting time before activation. The algorithm determines the dispersoid with the least waiting time. This dispersoid is then activated, the elapsed time is increased by an increment equal to this waiting time and the wait time for all other dispersoids is decreased by the same increment. Any true instabilities are allowed to take precedence over thermal events.

★Arbitrary combinations of obstacle strength and size are permitted. The intersection of each dispersoid with the slip plane is chosen to lie at a random position along the dimension of the dispersoid normal to the slip plane.

★Intersection, Orowan looping and diffusive climb mechanisms, together with thermally activated processes, are all permitted and form competing mechanisms in the model. Climb is simulated by assigning a wait period equal to the time required for Einsteinian diffusive drift over the shortest distance, normal to the slip plane, to the edge of the dispersoid.

★Duesbery-Sadananda (DS) line tension formalism is incorporated in the harmonic mean approximation.

a.2 Strength of Random Dispersions

The model can be used to calculate the athermal strength of random dispersions. This is of interest because it permits comparison of the predictions of the model with those of earlier, simpler approaches. Figure 2 shows the computed strengths of random dispersions as a function of critical breaking angle for a constant number density of dispersoids (i.e. constant mean separation) and three different dispersoid diameters. The unit of strength is the strength of a square array of point obstacles in the classical Friedel line tension approximation, that is, $\mu b/L$. This choice permits the primary strength dependence, on L^{-1}, to be factored out, thereby emphasiizing the influence of the different line tension models. The black curve in Figure 2 shows the behavior predicted by the current computer codes for Friedel line tension. This agrees

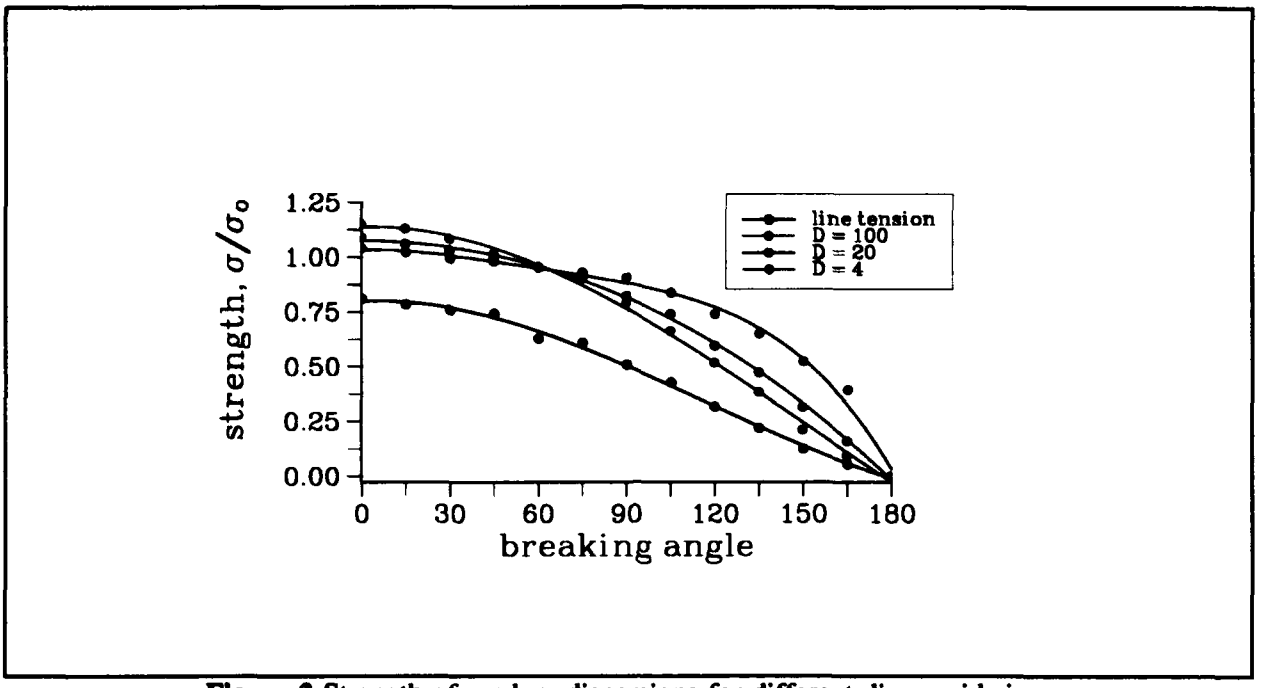

Figure 2 Strength of random dispersions for different dispersoid sizes

closely with the early calculations of Foreman and Makin[4] and serves to confirm the validity of the model. The remaining curves show the behavior for DS line tension for dispersoid diameters of 100b (blue curve), 20b (green) and 4b (red). Common to all the DS curves is a strength of

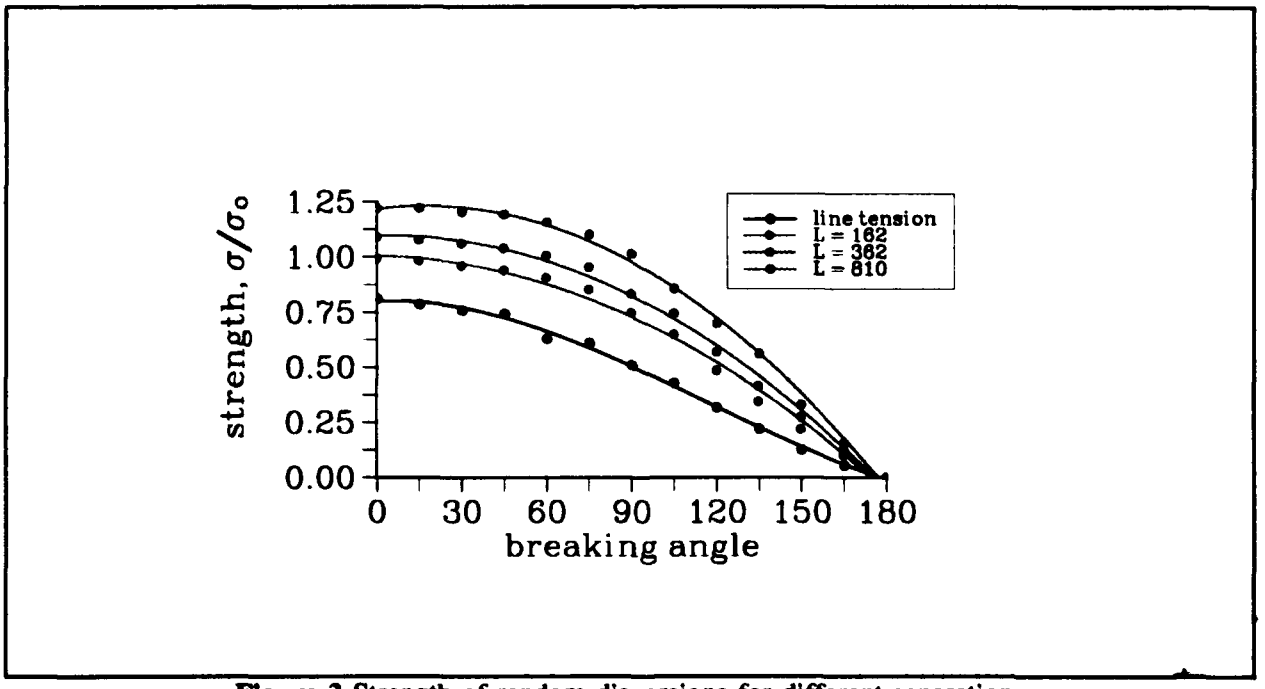

Figure 3 Strength of random dispersions for different separations

30% or more greater than the classical value. This is most noticeable for large breaking angles (weak dispersoids) and small diameters. In practical terms, this means that for small dispersoids, the intrinsic strength of the dispersoids is not of great consequence, provided that the breaking angle is less than about 120°. Figure 3 shows a similar strength plot, for a constant dispersoid diameter of 50b and for mean separations of 810b (red), 362b (green) and 162b (blue). Once again, it is evident that the more accurate DS line tension predicts strengths considerably in excess of that of the classical model.

a.3 Creep Lifetimes

The main purpose of the current model is the prediction of creep lifetimes. Using the novel algorithm described above, this has been done for a representative dispersion with volume fraction of 5% and dispersoid diameter of 100b. In a random arrangement, these values correspond to a mean apparent separation <L> = 324b and a mean intersected diameter <D> =

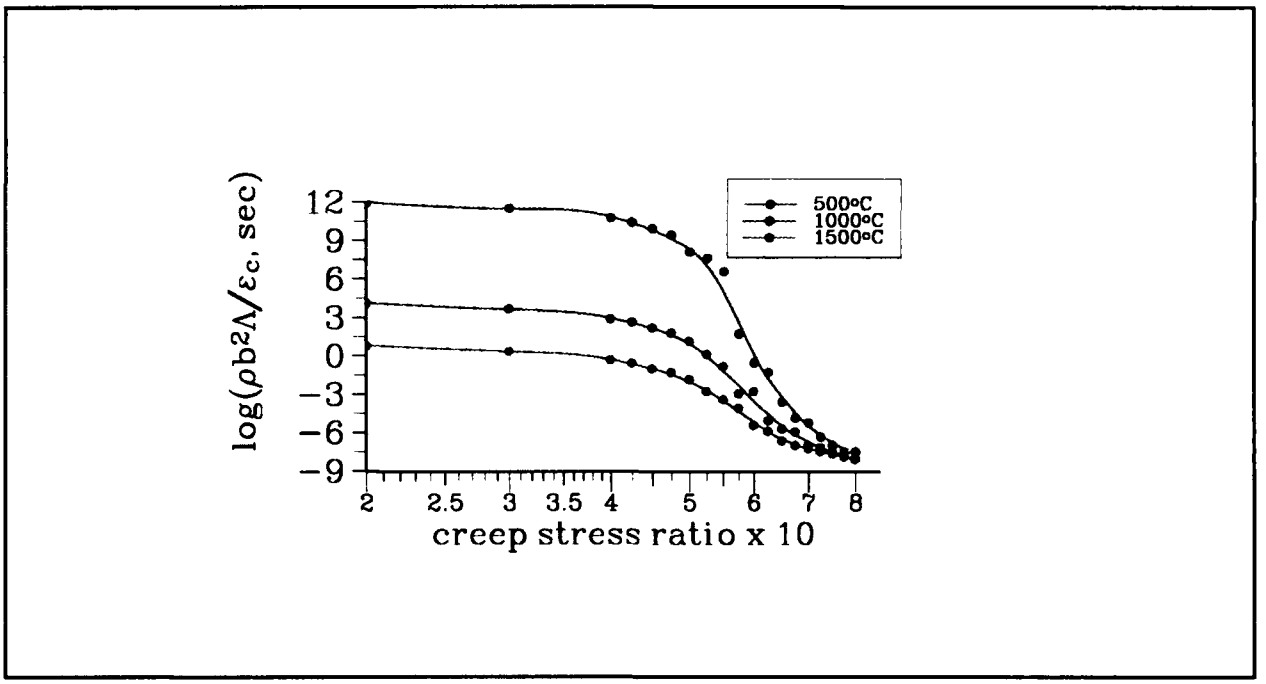

Figure 4 Creep lifetime as a function of creep stress ratio for a self-diffusion energy of 3eV (291KJ/mol)

78b. A breaking angle of 90° has been chosen as typical of many experimental measurements and theoretical simulations[1]. In Figure 3 is plotted the quantity $\log_{10}(\rho b^2\Lambda/\varepsilon_c)$ (which will be called the lifetime factor), where ρ is the dislocation density and Λ is the lifetime in seconds to a critical strain of ε_c, against the ratio of the creep stress to the athermal strength. The particular values in Figure 3 correspond to a ratio of $\rho/\varepsilon_c = 10^{10}$, as would be the case, for example, for a dislocation density of 10^8 cm^{-2} and a critical strain of 0.01. It can be seen from Figure 3 that the model can predict lifetimes over a range of 20 orders of magnitude. Each point is an average

of five calculations based on different random number sequences, and each calculation, taking 15-30 minutes on a fast personal computer, samples the creep motion of a single dislocation over a distance of 10^5b in a slip plane segment of width 10^4b. The three curves in figure 3 refer to temperatures of 500°C (red), 1000°C (green) and 1500°C (blue). There are three clear regimes. For high creep stress ratios, of order 0.75, the lifetime is very short. For creep stress ratios 0.65 to 0.5, the lifetime increases very rapidly, finally saturating into a low-index power law dependence for creep stress ratios of less than 0.45. The physical reasons for the three stages are as follows. At high creep stress ratios, the inter-obstacle spacing is given accurately by the mean apparent separation, and each successful thermal activation results in 10^2 - 10^3 secondary, mechanical activations (i.e. induced instabilities). In the transition region, the number of secondary activations drops rapidly. At the same time, the dislocation curvature decreases; consequently the true separation of the obstacles *along the dislocation line* increases, so that there are fewer activation sites. In the low-stress limit, the number of secondary activations saturates at < 1 and the true separation of obstacles approaches 3<L>.

These factors alone are insufficient to explain the curves in Figure 3 completely. The activation energies for overcoming the dispersoids by thermally activated glide can be very large, especially at low stresses. With glide processes alone, the lifetimes become extremely large. Observation of the development of the substructure indicates that the dislocations become 'stuck' on

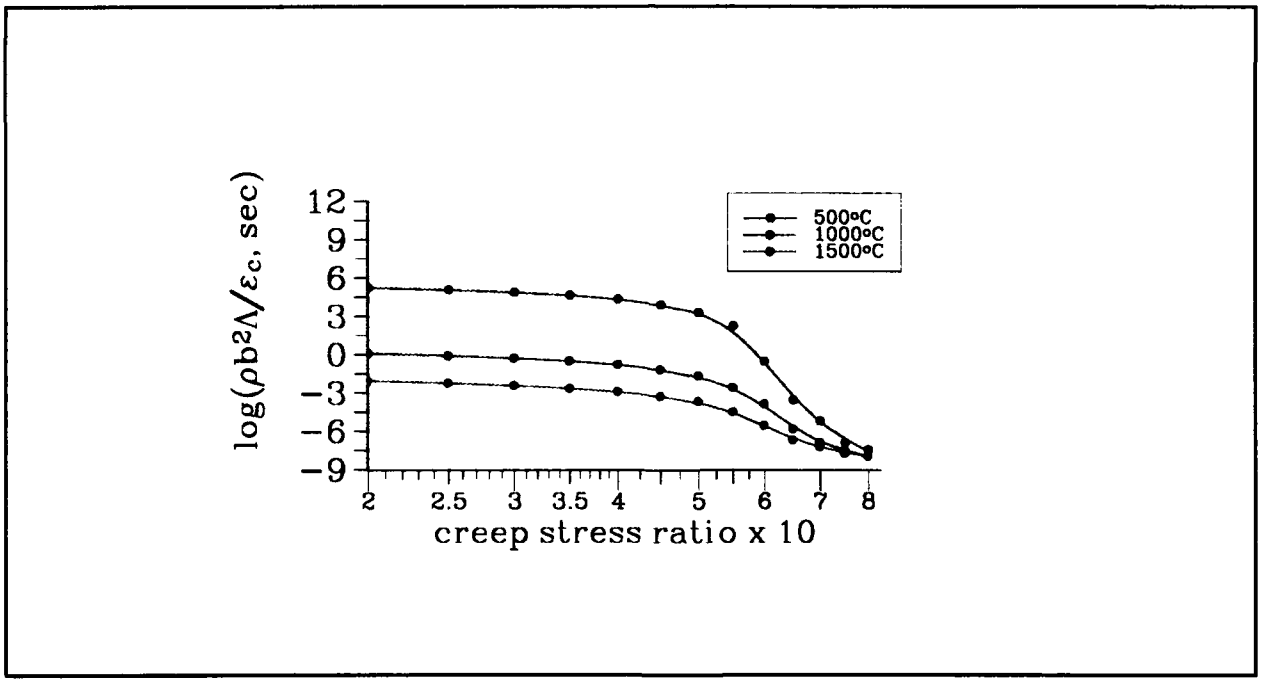

Figure 5 Creep lifetime as a function of creep stress ratio for a self-diffusion energy of 2eV (194KJ/mol)

sequences of "hard" obstacles. To keep the lifetimes at reasonable levels, it is necessary to allow for the overcoming of dispersoids by climb. In Figure 3, the self-diffusion energy, which governs the climb process, is set at 3eV (291KJ/mol). Figures 4 and 5 show the change in behavior when

self-duffusion energy is set to 2eV (194KJ/mol) and 1eV (97KJ/mol), respectively. The low-stress

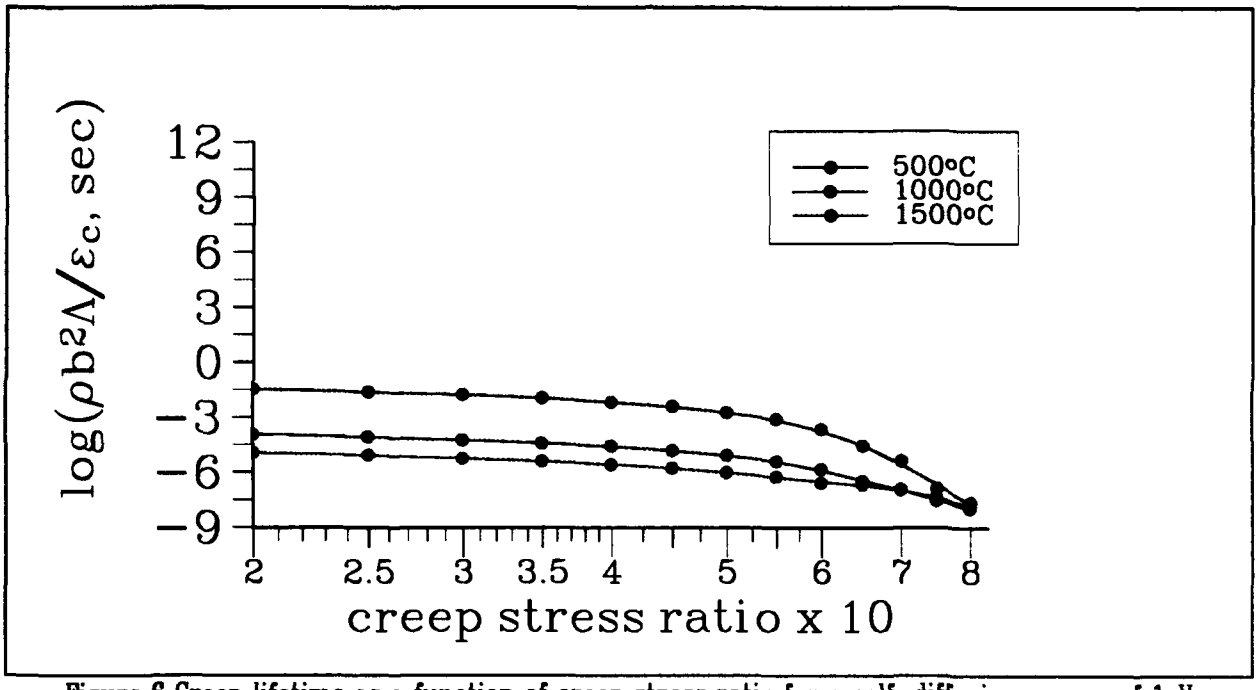

Figure 6 Creep lifetime as a function of creep stress ratio for a self-diffusion energy of 1eV (97KJ/mol)

lifetime factor at 500° C drops by 13 orders of magnitude as the self-diffusion energy drops from 3eV to 1eV, exactly as expected from a mechanism controlled by diffusion.

b. Comparison with experiment

The results reported above are "hot off the press" and as yet there has been no time to make the comparison with experiment.

c. Implications

★That low-stress creep is dominated by dislocation climb and hence by the self-diffusion energy.

★Long-term creep can be modelled by computer simulation, without the need for empirical extrapolation.

d. Plans *(given continued funding)*

★The results of the creep model will be compared both with experimental results and with the standard engineering formulae used to extrapolate long-term creep properties[5].

Task 200. Lifetimes of piezoelectric ferroelectrics

The utility of PZT as a 'smart material' is severely limited by its premature mechanical failure when subjected to cyclic loading. The cause of this failure forms the critical question. The central problem is that an irreversible mechanism is necessary to explain the experimental observations, while the overt physical properties - that is, piezoelectricity, ferroelectricity and ferroelasticity - are all symmetric to reversal. A theory will be presented which introduces an intrinsic irreversibility and, at the same time, explains all salient experimental observations.

The key experimenal observations are as follows.

⋆In the poled state, ferroelectric domains are elongated strongly in the direction of the poling field and are separated by walls with little curvature.

.

⋆Under cyclic mechanical loading at 70% of the monotonic fracture stress (140MPa), the lifetime is in excess of 10^7 cycles. At stress amplitudes from 75% to 95% of the fracture stress, the lifetime decreases sharply from 10^5 to 10^2 cycles)[6]. The effect of temperature is unknown.

⋆Under cyclic (resonant) electrical loading, the lifetime depends on temperature. For deformation above 80° C, failure is much more rapid than below this critical temperature. Predeformation below 80° C prior to high-temperature deformation leads to even more rapid failure. Damage is not detectable for deformation below 80° C, but is observed as intergranular cracking at higher temperatures[6].

a. Theory

a.1 Domain Wall Structure

There are two basic classes of domain wall in PZT and other ferroelectrics belonging to the perovskite family. The 180° wall separates domains in which the polarization is reversed, but the lattice remains commensurate. On the other hand, the polarization (which is always parallel to the tetragonal c-axis) changes by 90° on passage through a 90° domain wall, so that there is an incommensuracy where the c-axis on one side of the wall meets one of the a-axes on the other. In strictly geometric terms, the 90° wall is an interface between two crystals with different lattice constants. This is similar to the problem of an epitaxial layer on an incommensurate substrate and the physical consequences are well known[7]. For thin layers and small misfit, the incommensuracy is accommodated by coherency strains. As the thickness of the layer (or in the case of a ferroelectric, the domain width) increases, it becomes increasingly advantageous to concentrate the misfit into dislocations. With an approximate theory, Matthews[7] estimates the maximum misfit ϵ that can be accommodated by a layer of thickness h without instability toward dislocation formation as

so that, for example, dislocations would be preferred in a layer of thickness 100b if the misfit strain is greater than 0.0017. Therefore for PZT, for which the misfit is 1 - 3%, depending on the composition, dislocated domain walls are certainly to be expected. An example of a domain wall dislocation is shown schematically in Figure 7. In Figure 7 the wall is shown as a dashed line and the PZT unit cell is outlined at the top left of the figure. The dislocations will be regularly spaced along the domain wall and will have Burgers vectors which lie in the plane of the wall. Conservative motion will be possible only in the plane of the wall; the mobility of dislocations in the wall is uncertain, but will probably be low and thermally activated, as is usual for ceramic materials.

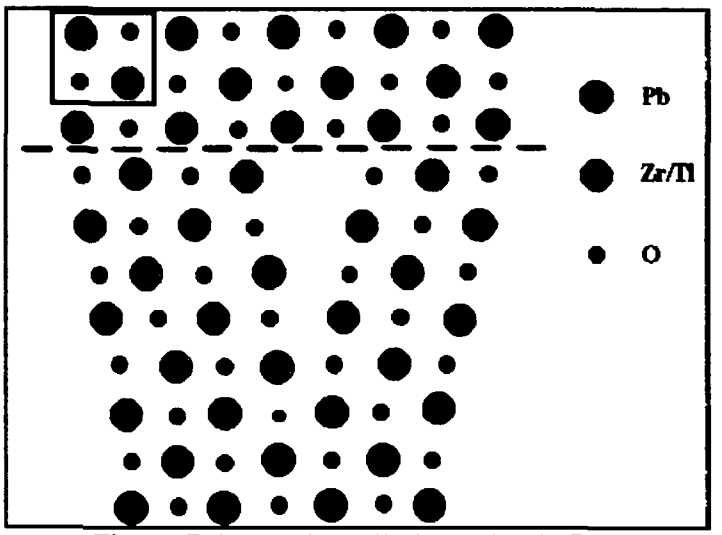

Figure 7 A domain wall dislocation in PZT

There are two sub-species of 90° domain wall. These are shown schematically in Figure 8, which shows unit cells of the structure on either side of the domain wall (green). The direction of polarization in the reference domain cell is indicated by a red-tipped arrow, that in the neighboring domain cell by a yellow-tipped arrow. The tetragonality is exaggerated for convenience. The two diagrams in Figure 8 show that the lattice in the neighboring domain can lie in two different orientations. In the upper diagram, the polarizing vector lies normal to the domain wall and there is misfit in only one of the two cell dimensions in the wall plane. A single set of dislocations suffices to relieve this misfit strain. In the lower diagram, the neighboring polarization vector lies parallel to the domain wall and there is misfit in both cell dimensions in the wall plane. To relievce this strain, two sets of dislocations, perpendicular to one another, are required. The description can readily be generalized. The upper diagram in Figure 8 describes what will be called a type I wall, which has one normal polarization vector. A type II wall has two parallel polarization vectors. In a first approximation, the type II wall, with double the density of dislocations, will have twice the energy of a type I wall. It can therefore be expected to occur only when geometrically necessary.

The domain wall structure is directly pertinent to domain wall motion, and therefore a few preliminary remarks are in order. The movement of a wall normal to itself requires transport of misfit strain. If the misfit has been concentrated into dislocations, dislocation climb, a non-conservative, thermally activated process involving the absorbtion or emission of vacancies, will be necessary. In this case wall motion will be relatively difficult, sensitive to temperature and

deformation rate. The climb process will be particularly difficult in PZT, because the vacancies must be emitted in pairs to maintain charge neutrality.

On the other hand, if the misfit is sufficiently small that coherent walls are favored, wall motion should be rapid and insensitive to temperature and rate. There is an intriguing possibility that both types of motion may occur. The misfit in PZT decreases with increasing temperature, so that a transition from dislocation-pinned walls to freely mobile coherent walls is quite possible. A transition of this type could explain the temperature dependence of cyclic failure in electrical cycling noted above. More detailed calculations and critical experiments are required to pursue this hypothesis.

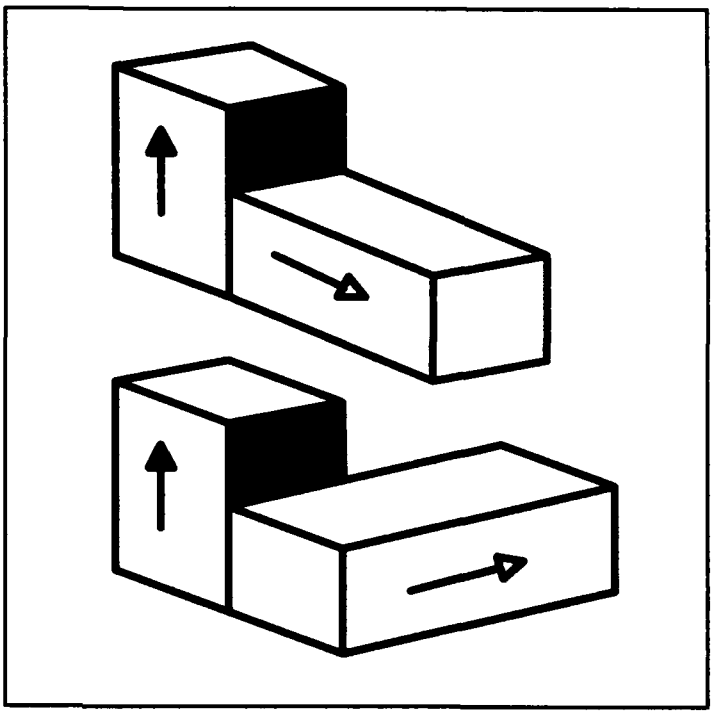

Figure 8 The two types of 90° domain wall

a.2 Domain Wall Motion

Because domain walls in ferro-electrics are stable (or, at least metastable) lattice defects, they do not couple directly to external fields, instead responding to thermodynamic forces - that is, to free energy gradients. In general, both electrostatic and mechanical terms must be taken into account. A simplified mean-field theory will be presented. Although crude, this theory demonstrates that there is a fundamental irreversibility which will lead to failure in cyclic loading.

There are two sources of internal energy - mechanical and electrostatic. Consider first the mechanical energy. The initial state is polycrystalline cubic PZT; a single grain will be treated. It is assumed that after transformation to the tetragonal structure the stresses within the grain are uniform. Then if a volume fraction f has its c-axis lying parallel to the z-axis of an external frame of reference which coincides with the axes of the original cubic structure, the elastic energy is given by

$$U_{el} = \frac{\mu}{4}\left(\frac{c}{a}-1\right)^2(1-f)\,(1+3f) \qquad (4)$$

where μ is the shear modulus and c, a are the tetragonal lattice constants. In the transformed state it is expected that the orientations of the tetragonal cells will be random, so that f = 1/3 and U_{el} is a maximum. For c/a -1 = δ = 0.017 (for composition close to the morphotropic phase boundary and a temperature of 298K[7]) and μ = 40GPa, U_{el} is about 4.42MJ/m^3.

After poling with an electric field along the z axis, the electrostatic energy can be estimated from the remanent polarization, P_r, which has a value[8] of $0.40C/m^2$ for the composition and temperature given above. Assuming that P_r is proportional to δ, the electrostatic energy is given by

$$U_{es} = \frac{1}{2}P_r.E = \frac{1}{2}f^2\frac{P_r^2}{\kappa\kappa_o} = \frac{1}{2}f^2\delta^2\frac{P_o^2}{\kappa\kappa_o} \qquad (5)$$

in which κ is the dielectric constant along the z axis (~ 1000) and κ_o is the permittivity of free space (= 8.8×10^{-12}F/m). The maximum electrostatic energy, from (5), of $9.0MJ/m^3$ is comparable with the maximum elastic energy.

The two terms (4) and (5) form contributions to the internal energy which change as domain walls move and therefore exert generalized forces on the walls, as

$$F_{el} = -\frac{\partial U_{el}}{\partial f}\frac{df}{dx} \qquad F_{es} = -\frac{\partial U_{es}}{\partial f}\frac{df}{dx} \qquad (6)$$

where x is measured normal to the domain walls and the poling axis, and is also the direction of tensile and compressive stress during mechanical load cycling.

The final force on the domain walls occurs when an external stress is applied. This is seen best by reference to Figure 9, which shows a type I domain wall (vertical line) separating domains with cell shape and polarization shown by rectangles and red-tipped arrows. For a tensile stress σ acting normal to the domain wall, a movement of the wall to the left through a distance dx causes the external stress to do work $-\sigma\delta dx$. Therefore there is a configurational force of $-\sigma\delta$ on the wall, as shown. Figure 9 also shows the sense of the forces F_{el} and F_{es}. For a compressive applied stress the force $\sigma\delta$ is reversed in sign, but the other forces remain unchanged.

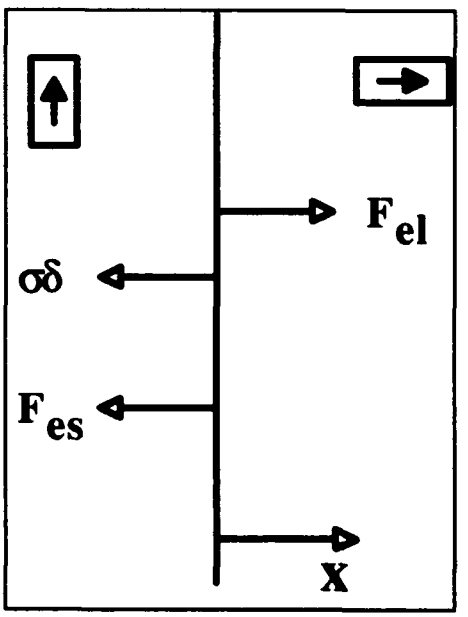

Figure 9 The forces acting on a domain wall

The essential irreversibility of domain wall motion stems from the imbalance of F_{el} and F_{es}. The resultant of these two forces maintains a constant bias while the external stress reverses during cyclic deformation. Converting all forces (per unit area) to units of μ, for ease of comparison

$$\frac{F}{\mu} = 1.50\delta^2(f-\frac{1}{3}) - 1.56\delta^2 f \mp \delta\frac{\sigma}{\mu} \qquad (7)$$

in which the terms on the right-hand side, in order, are due to the elastic energy, the electrostatic energy and the applied stress. The sign of the latter term is to be taken as negative for tension, positive for compression. Effectively

separated by walls with little curvature.

A domain wall which is normal to the electric field has a surface charge which experiences a force due to the field which promotes motion of the wall in the direction of the field axis. Walls interacts directly parallel to the field experience no such force. Hence domains tend to elongate parallel to the field axis, growing until terminated by the crystal surface or a grain boundary. The remaining walls are constrained by misfit dislocations to maintain long-range linear form. At the short range, curvature of the walls, which will be low-energy type I walls, requires formation of small segments of type II walls, and is therefore inhibited.

★*Under cyclic mechanical loading at 70% of the monotonic fracture stress (140MPa), the lifetime is in excess of 10^7 cycles. At stress amplitudes from 75% to 95% of the fracture stress, the lifetime decreases sharply from 10^5 to 10^2 cycles)*[6]*. The effect of temperature is unknown.*

As the crystal depoles by domain wall movement, the domains lengthen in a direction parallel to the stress axis and shorten in the poling direction. This creates cracks at the grain boundaries which lengthen systematically during cyclic stressing, due to the intrinsic irreversibility of domain wall motion, until a crack of critical length is created and fracture occurs. This process is strongly dependent on temperature and stress, because the controlling mechanism is dislocation climb.

★*Under cyclic (resonant) electrical loading, the lifetime depends on temperature. For deformation above 80° C, failure is much more rapid than below this critical temperature. Predeformation below 80° C prior to high-temperature deformation leads to even more rapid failure. Damage is not detectable for deformation below 80° C, but is observed as intergranular cracking at higher temperatures*[6].

There is a critical temperature above which dislocations will be expelled from the domain walls and wall motion will take place more easily. Cyclic deformation above this critical temperature, will lead to immediate formation of large cracks, hence to rapid failure. Cyclic deformation below the critical temperature involves much smaller wall motions, causing microcracks of a size below the detection limit. However, if a predeformed specimen is subsequently deformed above the critical temperature, the microcracks will rapidly coalesce to form larger cracks.

c. Implications

★The irreversibility which leads to failure of PZT in cyclic stressing is linked with the motion of ferroelastic domain walls. A bias towards the direction of wall motion which favors depoling results in a ratchet mechanism. This leads to grain boundary stresses which increase steadily until cracks form and the material fails.

d. Plans

★Ferroelastic domain wall motion will be modelled, below and above the critical misfit

temperature. Lifetimes will be calculated and linked to measurable parameters. Critical questions will be answered: specifically, can lifetimes be lengthened by bias electric or stress field stabilization?

★Confirming experiments will be suggested to White at NIST and Sadananda at NRL.

References

1. M.S. Duesbery and N.P. Louat, November 1992 ONR report.
2. M.S. Duesbery and K. Sadananda, Phil. Mag., 63 (1991) 535.
3. D.J. Bacon, U.F. Kocks and R.O. Scattergood, Phil. Mag. 28 (1973) 1241.
4. A.E. Foreman and M.J. Makin, Phil. Mag. 14 (1966) 911.
5. R. Viswanathan, *Damage Mechanisms and Life Assessment of High-Temperature Components*, ASM International, Metals Park, Ohio, 1989.
6. G. White, NIST, private communication.
7. M. Fukuhara, A.S. Bhalla and R.E. Newnham, Phys. Stat. Sol. (a) 122 (1990) 677.
8. L.E. Cross and K.H. Härdtl, Encycl. Chem. Technol., 1980, reprinted in *Piezoelectricity*, AIP press, 1992, p2.

Appendix

Analytical Treatment of the Strength of Random Dispersions

Abstract: The methods of Boltzmann's classical statistical mechanics are employed to calculate the yield strength in the absence of thermal activation in the case where hardening is due to randomly dispersed spherical particles.

Introduction

We seek to determine the yield strength at 0 K of a material hardened by the presence of spherical particles which act as simple blocks to the motion of dislocations. The analysis is based on a consideration of the stability of a sequence of lengths of a single dislocation which has impinged on spherical particles in the process of traversing a slip plane.

Analysis

We assume:
that when acted on by a uniform stress σ, dislocations are bent into arcs of circles of radius R,

$$\sigma = \frac{\mu b}{R}. \qquad (1)$$

where μ is the shear modulus and b the magnitude of the Burgers vector;
that impenetrable particles of shear modulus μ are randomly distributed and provide restraining forces, F, of magnitudes which are related through the breaking angles $\alpha(a)$ to the radii (a) of the circles of intersection between particles and slip planes and which are specified by

$$F = \mu b^2 \sin \alpha(a)$$

and;
that the yield stress is the largest for which it is possible to have a stable dislocation join an infinite number of particles along a line which is essentially straight and hence does not cross itself.

Towards the determination of this stress we shall adapt the theoretical analysis first introduced by Hanson and Morris [1] and subsequently modified and employed by Labusch [2] and by Louat (3) to determine the yield strength due to a dispersion of point obstacles all of which provide the same maximum restraining force,

$$F \sim \mu b^2 \sin\alpha \sim \alpha \mu b^2 \qquad (3)$$

This analysis rests on the rolling circle technique employed by Foreman and Makin [4] in their numerical investigation of this hardening. Thus, it was argued (see

fig. 1) that a dislocation stable at a sequence of positions - - -,k-2, k-1, will be also be stable at the next position k provided the particle associated with the k+1th particle is centered anywhere in the region traversed by a rolling circle as shown hatched; this region is bounded by an angle $\theta \leq 2\alpha$. A particular characteristic of such sequences of dislocation lengths is that they must not cross themselves.

Here, we shall adapt the treatment of Hanson and Morris [1] to the case where the strength of a particular obstacle depends on the radius of the circle of intersection between the spherical particle concerned and the slip plane. To proceed, we note first from fig (1), in the case of point obstacles, that, following the path of a rolling circle, the angle turned between successive tangents, t_k, is equal to the angle,ϕ, which gives the direction of the trailing circle edge at the point of rotation (see fig (2)). It is then readily seen that in the case of an obstacle with radius , a, the angle turned becomes:

$$\overline{\Phi} = \phi \ (\ 1 + a \ / \ R \ ) \equiv T\phi$$

Then, if the number of points be N and if the angle ϕ occurs n_i times we have

$$N = \sum_{i=1}^{n} n_i \qquad (3)$$

and the total angle turned is

$$\sum_{i=1}^{n} n_i \, \overline{\phi_i} = \Phi \qquad (4)$$

If N is indefinitely large, but Φ finite, the average value of ϕ_i is zero. In this case the whole dislocation line is either straight or contains equal infinities of complete clockwise and anticlockwise rotations. The latter configuration is a situation of low probability which we can neglect.

The procedure for the determination of the thermodynamic probability is akin to that employed to determine the Maxwell-Boltzmann distribution of kinetic energies in an ideal monatomic gas. Thus, if there are n partitions at each of N points the thermodynamic probability that the ith is employed n_i times is:

$$P = \frac{(N \ !) \prod_{i=1}^{n} p_i^{n_i}}{\prod_{i=1}^{n} n \ !} \qquad (5)$$

where p_i is the occupational probability of the ith region. To determine p_i we divide the hatched area ,A, into n regions of area, δA_i (i = 1 ,n) each characterized by a value of ϕ, say ϕ_i and see that when the concentration of second phase particles is C and provided the area ΔA_i is sufficiently small, the probability that a point k lies in a particular area ΔA_i is:
Here, we have expressed C in terms of the volume fraction, f, of second phase. Thus, the number, M, of particles per unit volume is such that

$$p_i \equiv 1-e^{-C\Delta A_i} = 1-e^{\frac{-3\pi f \Delta A_i}{2\pi r^2}} \sim C\Delta A_i \qquad (6)$$

$$\frac{4\pi r^3 M}{3} = f.$$

So that the concentration, C, of circles of intersection of particles by a slip plane is

$$C=2r\,M = \frac{3f}{2\pi r^2}.$$

On the basis that the most probable configuration of a system having a large number of parts is that which actually occurs we have, to determine this configuration, only to maximize P subject to the constraints offered by (3) and(4). To proceed we take advantage of the facts that N and n_i are both large to employ Stirling's approximation for the factorial and then set the variation in ln P to zero. We find:

$$\delta \ln p = \sum_{i=1}^{n} \delta n_i + \ln p_I - \sum_{i=1}^{n} \ln n_i$$

while (3) and(4) become:

$$\sum_{i=1}^{n} \delta n_i = 0, \qquad (7)$$

$$\sum_{i=1}^{n} \delta n_i \overline{\phi_i} = 0. \qquad (8)$$

Whence introducing the Lagrangian multipliers λ and γ we have

$$\ln p_i - \ln n_i + \gamma + \lambda\overline{\phi_i} = 0$$

so that

$$n_i = \frac{N p_i e^{\lambda_i}}{\sum_{i=1}^{n} p_i e^{\lambda \phi_i}} \qquad (9)$$

Then from (4) and (8) we have so that we find on substituting for n_i in the logarithm of P and after some manipulation:

$$N\sum_{i=1}^{n} e^{\lambda\phi_i}\,\phi_i\,p_i = \Phi\,S,$$

where

$$\sum_{i=1}^{n} \phi_i e^{\lambda\phi_i} = S. \qquad (10)$$

$$P = S^N e^{-\lambda\phi} \qquad (11)$$

$$P = S^N\, e^{-\lambda\Phi}. \qquad (11)$$

Then invoking (6) and (9) and proceeding to the limit of small quantities δA, (10) becomes:

$$P = e^{-\lambda\Phi}\ [\ c\int e^{\lambda\overline{\phi}}\,dA]^N$$

We have now to determine S and λ. Here, where A is the area indicated in fig.(1) we have, for $1/2R<<1$:

$$S = C\int_0^{2R} (1+r)\,dl \int_{T(\arcsin l/2R)}^{T(2\alpha-\arcsin l/2R)} e^{\lambda\phi}d\phi$$

$$\sim \frac{C\,R^2T\,(e^{2\alpha\lambda T}-1)}{\lambda}\,\frac{(1+e^{-\pi\lambda T})}{(\lambda T)^2+1} \qquad (12)$$

The determination of λ is assisted by the realization that

$$\frac{d\,\ln S}{d\lambda} = \frac{1}{S}\,\frac{dS}{d\lambda} = \sum_{i=1}^{n} \frac{\phi_i e^{\lambda\phi_i} p_i}{S} = \frac{\Phi}{N} \to 0 \ \text{as}\ N \to \infty \qquad (13)$$

and λ must be such that

$$\frac{dS}{d\lambda} = 0.$$

This question can only be resolved numerically. In the special and unrealistic case in which $\alpha << 1$ we find, independent of the value of T, that $\lambda = 1.41 / \alpha$. In comparison with the case treated previously [1] there are additional complications: the obstacles have finite radius and; because the radii of individual obstacles differ one from the another, they have variable strengths. We shall now explore the nature of this variation. Bacon ,Kocks and Scattergood [4] have shown through numerical studies that the Orowan stress,τ, for a linear sequence of impenetrable circular blocks to dislocation motion having radius a

and inter-center spacing L is given by:

$$\tau = \frac{\mu b}{4\pi} \frac{\ln(\frac{X}{b})}{(L-2a)}$$

where,

$$\frac{1}{X} = \frac{1}{2a} + \frac{1}{L}. \qquad (14)$$

Thus, the specific strength of these obstacles is variable and denoted by the term:

$$\frac{\ln(X)}{4\pi} = \sin \alpha. \qquad (15)$$

Here, the obstacles are not distributed along a straight line nor are they regularly spaced. Additionally their strengths are variable. The consequences of the first two particulars have been considered in the foregoing, we now examine the consequences of the variation in specific strength.

To progress we suppose that the particles are spherical of radius r and that the concentration of the particulate phase is f. We then find that the mean spacing between particle centers in a slip plane is

$$l = \sqrt{\frac{2\pi}{3f}}\, r$$

Again, the mean value of the radius of intersection of such a plane with the particles is readily found to be:

$$(\frac{2}{3})^{\frac{1}{2}} r.$$

Then towards the evaluation of the quantity defined in (15) we follow Friedel and suppose that at yield, dislocation are bent into arcs of circles of radius R such that the areas swept by the dislocation in circular segments between obstacles contain about one obstacle. Taking the critical angle turned by the dislocation at an obstacle as 2θ, the area of a segment is:

$$\frac{4R^2\theta^3}{3}.$$

Thence we see that

$$\frac{4R^2\theta^3 f}{3} \sim \frac{(L-2a)^2\theta f}{3} = \frac{2\pi r^2}{3}.$$

so that

$$\frac{L-2a}{a} \sim \sqrt{\frac{\pi}{f\theta}}$$

and

$$L = a\,(2+\sqrt{\frac{\pi}{f\theta}}).$$

Thus, the mean value of the quantity X/b defined in (14) is

$$\frac{2r}{b}$$

and provided, as is usually the case, $f\theta < \approx 0.1$,
(15) becomes

$$\frac{\ln(\frac{2r}{b})}{4\pi} = \sin\alpha$$

Importantly in the circumstances considered here, the strength of a particular obstacle of radius a is denoted by

$$\alpha_i \sim \sin\alpha_i = \frac{\ln\frac{2a}{b}}{4\pi}; \qquad (16)$$

$$\alpha < \sim 60°.$$

An immediate consequence of these conclusions is that the radius R >>a since it is significantly larger than L unless $\theta > 60°$.

We are now in a position to consider the consequences of the simultaneous existence of obstacles of differing strengths. Reference to (12) and the realization that the analysis which proceeds it, is essentially linear in the concentration of obstacles, shows that we may define a parameter S_j for each group of obstacles characterised by a strength α_j and a concentration c_j and then consider the quantity:
which in the limit of a continuous distribution of obstacle sizes becomes:

$$S_o = \frac{R^2 \sum_{j=1}^{m} C_j (e^{2\alpha_j T\lambda} - 1)}{\lambda(\lambda^2 T + 1)}$$

$$S_o = \frac{R^2}{\lambda(\lambda^2 T+1)} \int_0^{\alpha_m} C(\alpha)\,(e^{2\alpha\lambda T} - 1)\, d\alpha. \qquad (17)$$

where α_m is the maximum strength of any obstacle, and C_α is the concentration of obstacles of strength α.

In the case under consideration where the particles are spherical and all of the same radius, r, it is easily shown that the fraction, f(a) of circles of intersection of having radii in the range a to a $+\delta a$ is

$$C(a)\,\delta a = \frac{a}{r\sqrt{r^2 - a^2}}\,\delta a.$$

and substituting for α in terms of a, (17) becomes:

$$S_0 = fr\frac{R^2}{4\pi r\lambda)} \int_0^r \frac{(\frac{2a}{b})^{\frac{(1+a/R)\lambda}{2\pi}} - 1}{\sqrt{r^2 - a^2}\ (\lambda^2(1+a/R)+1)}\, da,$$

where 2fr is the concentration of obstacles in a plane.

To progress, we observe that r/R is small and that the integral, I, lies between lower and upper bounds. Thus,

$$\frac{fR^2}{8\lambda(\lambda^2+1)} \int_o^r \frac{(\frac{2a}{b})^{\frac{\lambda}{2\pi}}}{\sqrt{r^2 - a^2}}\, da$$

$$< S_0$$

$$< \frac{fR^2 (\frac{2a}{b})^{\frac{r}{2\pi R}}}{8\lambda(\lambda^2+1)} \int_0^r \frac{(\frac{2a}{b})^{\frac{\lambda}{2\pi}}}{\sqrt{r^2 - a^2}}\, da. \qquad (18)$$

The integral I can be expressed in terms of the Beta function. Thus, we find: The interpretation of this result is assisted by the use of Stirling's approximation:

Whence we find that (19) is:

$$\int_0^r \frac{(\frac{2a}{b})^{\frac{\lambda}{2\pi}}}{\sqrt{r^2-a^2}}\,da = 2^{\frac{(\lambda-\pi)}{\pi}}\, r^{\frac{\lambda}{2\pi}} B\left(\frac{\lambda+2\pi}{4\pi}, \frac{\lambda+2\pi}{4\pi}\right). \qquad (19)$$

$$\Gamma(z) \sim 2\pi^{\frac{1}{2}}\, e^{-z}\, z^{z-\frac{1}{2}}.$$

$$I \sim \frac{2\pi\, 2^{(\frac{1}{2}-\frac{\lambda}{2\pi})}}{(\lambda+2\pi)^{\frac{1}{2}}}.$$

and that the inequality (18) becomes:

$$\frac{R^2\, C\, r^{\frac{\lambda}{2\pi}}}{2\sqrt{\lambda+2\pi}\;\lambda(\lambda^2+1)}$$

$$< S_0$$

$$< \frac{R^2\, C\, r^{\frac{\lambda}{2\pi}+\frac{r}{2\pi R}}}{2\sqrt{\lambda+2\pi}\;\lambda(\lambda^2+1)}$$

Inspection shows that these bounds are nearly coincident so that we may concentrate our attention on the simpler of the two.

Towards the determination of λ we have as indicated earlier:

$$\frac{d\,\ln S_0}{d\lambda} = \frac{1}{S_0}\,\frac{dS_0}{d\lambda} = \frac{\sum_{i=1}^{n} \phi_i e^{\lambda\phi_i} p_i}{S_0} = \frac{\Phi}{N};$$

a quantity which tends to 0 as N tends to infinity.

$$\frac{dS_0}{d\lambda} = 0$$

Accordingly differentiating with regard to λ we find that we require

$$\frac{1}{2\pi} \ln\frac{r}{b} - \frac{1}{\lambda+2\pi} - \frac{2\lambda}{\lambda^2+1} - \frac{1}{\lambda} = 0.$$

In the range of interest in which

$$10^2 \leq \frac{2r}{b} \leq 10^5$$

we find that

$$2 \geq \lambda \geq 1.$$

Finally we require as a condition for yield that $S_0 = 1$. Accordingly setting

$$R = \frac{\mu b}{\sigma}$$

in (12) and substituting for C in terms of f we have

$$\sigma^2 = \frac{3\mu^2 b^2 f (\frac{2r}{b})^{\frac{\lambda}{2\pi}}}{4\pi\, r^2\sqrt{\lambda+2\pi}\;\lambda(\lambda^2+1)}$$

Since λ is largest when r is least we find that there is little variation in the term $(2r/b)^{\lambda/2\pi}$ with variation in λ. Overall, for a constant value of f, the yield stress varies nearly with the inverse of the particle size. It may be noted that Freidel's [4] conclusion that stress varies with the square root of concentration is retained.

Conclusions:

An analytical analysis which proceeds on the same lines as those previously employed to evaluate the hardening effect of a dispersion of point obstacles has been used to deal with the case where the particles have finite radius. Qualitatively, the principle conclusions are that the predicted hardening should increase with the square root of the concentration of particulate phase and approximately with inverse of the particle diameter.

References:

1. Hanson, K. and Morris,J.W., J. Appl. Phys., 46, 983 (1975).
2. Labusch,R., J. Appl. Phys.,48, 4550 (1977).
3. Louat, N. ICSMA 5, 961 (1979).
4. Foreman, A.J.E. and Makin, M.J., Phil. Mag., 14, 911 (1966).
5. Bacon, D. J., Kocks, U.F. and Scattergood, R.O., Phil. Mag., 28, 1241 (1973).
6. Freidel, J., Les Dislocations, Gauther- Villiers, Paris (1956).

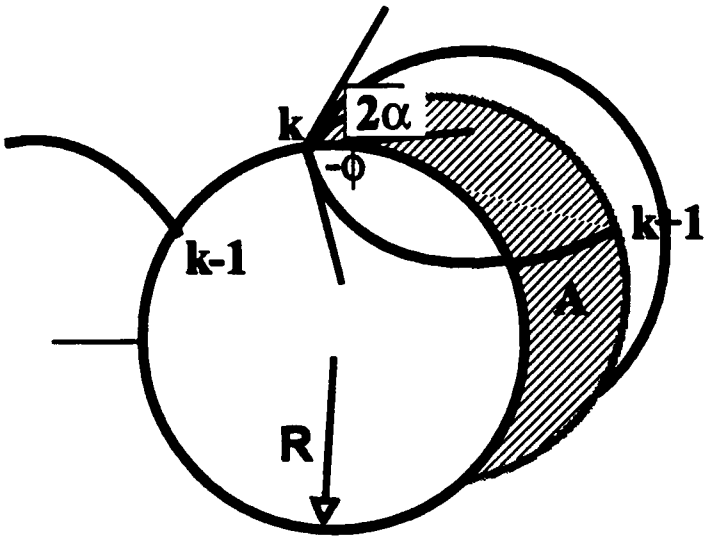

FIG. 1